A Model for the Correction of Surface Wind Data for Sheltering by Upwind Obstacles

PETER A. TAYLOR

Department of Earth and Atmospheric Science, York University, North York, Ontario, Canada

JAMES R. SALMON

Zephyr North, Burlington, Ontario, Canada

(Manuscript received 11 January 1993, in final form 14 April 1993)

ABSTRACT

Wakes behind 2D fences and 3D obstacles are reviewed with special emphasis on reduced mean wind speeds and sheltering effects. Based partly on Perera's study of wakes behind 2D fences, and assuming a Gaussian spread for wakes behind 3D obstacles, a shelter model is proposed and tested. The shelter produced depends on a wake moment coefficient $\tilde{C}_h$, which appears to be significantly less for 3D obstacles than for 2D fences. The model provides a simple basis on which to "correct" anemometer data for sheltering effects associated with upstream obstacles. Such corrections are an important step in the generation of improved surface wind climatologies and wind atlases.

1. Introduction

Although an ideal anemometer installation would be in flat, open terrain with no local obstructions, such sites are often difficult to find and compromises have to be made. As a result, wind measurements may be affected by both local topography and by modifications to the flow caused by the sheltering effect of upwind hedges, fences, trees, and buildings. In the production of a wind atlas for a region one would like to minimize or remove these site-specific effects. Impacts of local topography can be addressed through the use of models such as MS-Micro (Salmon 1987) or WASP (Wind Atlas Analysis and Application Program, Mortensen et al. 1993). The WASP suite of models also includes a shelter algorithm, which we will refer to here as WASP-SHELTER. The present paper proposes a new scheme to estimate sheltering effects. It has some common bases with the WASP-SHELTER model but pays more attention to differences between 2D and 3D obstacles and provides output with higher angular resolution.

2. Wakes behind surface-mounted obstacles

Hosker (1984) and Taylor (1988) review issues pertaining to the drag on surface-mounted obstacles and the evolution of the far wake region behind them. For the case with flow perpendicular to 2D fences of height h and porosity φ most of the work on the far wake behind 2D obstacles assumes that the velocity reduction u relative to the undisturbed, upstream profile $U_0(z)$ has a self-preserving form,

$$\frac{u}{U_0(h)} = \left(\frac{x - x_0}{h}\right)^{-1} G(\zeta), \tag{1}$$

where

$$\zeta = \left(\frac{z}{h}\right)\left(\frac{x - x_0}{h}\right)^{-a}. \tag{2}$$

Here, x is the distance downwind from the obstacle; x_0, often taken as zero, is the effective origin for the wake; and a is a constant that needs to be determined. The assumed x^{-1} power law, or very close to it, for the downwind decay of u with x is predicted by all the theories considered by Taylor and is consistent with all of the wind tunnel and field data that he reviews. There is more variability in the value of the coefficient a, which ranges from near 1 in some theories (e.g., Townsend 1965) to values near 0.5 in others and in most of the observational data. One possible reason for this discrepancy could be that the measurements have been made at downwind distances from the obstacle, which are not large enough for far wake conditions and the final self-preserving or similarity form solutions to apply. Many of the published data for 2D obstacles [e.g., Seginer and Sagi (1972), Counihan et al. (1974), Arya and Shipman (1981), Perera (1981)] are for downwind distances in the range $10h$–$50h$. At larger distances the velocity wake becomes weaker and

Corresponding author address: Dr. Peter A. Taylor, Department of Earth and Atmospheric Science, York University, 4700 Keele Street, North York, Ontario, Canada M3J 1P3.

may spread beyond the constant stress region. Also, in wind tunnel studies, downstream development of the basic boundary layer may be taking place, making it harder to isolate u from $U_0(x, z)$. Data for x/h of order 10–50, are, however, quite convincing when presented in normalized coordinates [see, for example, Arya and Shipman (1981), Fig. 13; Perera (1981), Fig. 5].

The wake model of Counihan et al. (1974), hereafter referred to as CHJ, gives $a = (n + 2)^{-1}$, where n is the coefficient in an assumed power law for the U_0 profile. CHJ take $n = 0.125$, based on their experimental mean velocity profile and thus $a = 0.47$. Perera's (1981) measurements confirm several aspects of the CHJ theory and his empirical formula, which provides the foundation for the WASP-SHELTER model, incorporates this expression for a.

There are fewer published results available for velocity perturbations in the far wake behind 3D obstacles and most are for solid obstacles ($\varphi = 0$). We will assume that the same far wake behavior would apply to porous obstacles, such as trees or bushes. We will also assume here that the obstacle of height h is "surface mounted" but we should note that some trees and wind turbines may provide most of their flow obstruction at heights away from the surface (c.f. Taylor 1980).

One of the most detailed studies of wakes behind 3D surface-mounted obstacles in a turbulent boundary layer that we are aware of is that conducted by Lemberg (1973) and reported in his University of Western Ontario Ph.D. thesis. Lemberg's results, in the range $5 < x/h < 20$, for the wake behind a variety of obstacles suggest,

$$\frac{u}{U_0(h)} = \left(\frac{x}{h}\right)^c f(\eta, \zeta) = \left(\frac{x}{h}\right)^c F(\eta)G(\zeta), \quad (3)$$

where $\eta = (y/h)(x/h)^{-b}$ and $\zeta = (z/h)(x/h)^{-a}$. Here z is the vertical axis normal to the wall and y is the horizontal axis normal to the mean flow. We estimate values of $c = -1.6$ and $a = b = 0.5$ based on this work. Arya and Gadiyaram (1986) also found $c = -1.6$ with a between 0.35 and 0.5 for conical obstacles, while Hunt (1971) predicted $c = -1.5$. Several CSU (Colorado State University) wind tunnel studies in both neutral and stable boundary layers (e.g., Woo et al. 1976; Kothari et al. 1979) extend to distances of order $60h$. They find c values varying from -1 to -2, depending on building shape and boundary-layer stability. The neutral boundary-layer data in typical ranges from $3h$ to $30h$ are generally consistent with a value of -1.5. We should remark that we are considering only the "momentum wake," rather than the "vortex wake" (c.f. Hansen and Cermak 1975; Hosker 1984). The presence and persistence of vortex wakes is highly case specific and is beyond the scope of the present analysis. We can, however, comment that strong longitudinal vortices often give velocity increases in part of the wake region as a result of downward entrainment of fast-moving air into the wake, that these velocity excesses decay slowly [as $(x/h)^{-1/2}$, see Hosker (1984)], that meandering of trailing vortex wakes in a highly turbulent boundary layer will lessen their average impact, and that vortex wakes will probably be most important in stably stratified, low turbulence flows past obstacles situated on relatively smooth surfaces. When present, these vortices could lead to local velocity perturbations that depart significantly from the estimates of our sheltering model.

Note that integrating (3) with respect to y yields the result

$$\int_{-\infty}^{\infty} u dy \sim x^{b+c} G(\zeta) \int_{-\infty}^{\infty} F(\eta) d\eta = x^{b+c} G(\zeta) \quad (4)$$

if the integral of F is set equal to unity. In a far wake model with linearized perturbation equations, the cross-stream integrated equations for a 3D wake are the same as the equations for a 2D wake (Taylor 1980). We will require this of our simple model. In the near wake region, turbulence will be modified in a nonlinear way and wakes could be significantly different in 2D and 3D cases. This factor is accounted for in our model by differences in the wake strength coefficients.

For wakes behind wind turbines, several models, for example, the Risø model discussed by Katic et al. (1986), assume a linear spread of the wake, that is, $a = b = 1$. This spread has an analog with that of a conservative tracer or pollutant plume in a uniform mean flow where, close to the source, the cross-stream spread σ_y predicted by the statistical theory of diffusion is proportional to x, (see e.g. Hanna et al. 1982). For the far wake the same statistical theory would correspond to $a = b = 0.5$.

Although the evidence is clearly not completely consistent, we will base our sheltering model on a self-preserving form for velocity perturbations in the wake behind a 3D obstacle of the form given by Eq. (3) above with $c = -1.5$, and $a = b = 0.5$. We adopt this knowing it to be inconsistent with some theories of linearized boundary-layer wakes but noting the success of the CHJ model and its consistency with the mean velocity observations of 2D and 3D wakes in both wind tunnel and field studies. For a 2D wake, integration of Eq. (3) gives Eq. (1) with $a = 0.5$. The CHJ theory and the empirical equation for 2D wakes proposed by Perera (1981) and used in the WASP-SHELTER model have $a = 0.47$ but, for the range of x/h with which we will be most concerned, the difference will be small. We prefer the 0.5 value for symmetry and simplicity.

In the shelter model to be proposed below, the function F represents the lateral velocity deficit variation in the wake. Simple intuition, Hunt's work (see Hosker 1984), and Lemberg (1973) all suggest a Gaussian spread, given by

$$F(\eta) = \frac{1}{(2\pi)^{1/2} a_f} \exp\left(\frac{-\eta^2}{2a_f^2}\right), \quad (5)$$

although, as Hosker (1984) and others remark, the agreement with data is "at best fair." In our notation, $\eta = (y/h)(x/h)^{-1/2}$. The integral of F with respect to η from $-\infty$ to $+\infty$ is equal to 1.0 and the corresponding wake width, $\sigma_y = a_f(xh)^{1/2}$.

Lemberg presents wind tunnel results for the wake behind a cube (his S4 case) in a plot of $\ln[-\ln(u/u_{cl})]$ versus $\ln[y/(xh)^{1/2}]$, where u_{cl} is the centerline velocity perturbation ($y = 0$) at the height z/h and downwind position x/h being considered. Note that $u/u_{cl} = F(\eta)/F(0)$. There is still considerable scatter. Lemberg's theoretical prediction corresponds to $a_f \approx 0.3$ but many of the data at heights of order $h/2$ would be better matched by taking $a_f = 0.4$ or 0.5. The plots of lateral variation given by Castro and Robins (1977, Fig. 9) are for $z/h = 0.5$ and at locations close to the body. Their data for $x/h = 3$ and for the cube mounted both normally and diagonally, show an approximately Gaussian spread for the velocity deficit and correspond to $a_f \approx 0.5$. This value is also compatible with most of the data presented by Hunt (1974) and reviewed by Hosker (1984, Fig. 7.27) although it would give a line lying slightly to the right of the "best fit"—which corresponds to $a_f = 0.34$.

It might be argued that a_f should be dependent on surface roughness and, perhaps on obstacle shape. We have no data on this, however. In the WEMOD shelter model to be discussed below, we assume a Gaussian lateral spread and that a_f is a "user specified" parameter. Our recommendation is to set $a_f = 0.5$.

3. The drag, the couple, and the wake moment for surface-mounted obstacles

In the far wake behind an obstacle in a uniform flow with velocity U_0, the momentum deficit

$$q = \int_{-\infty}^{\infty} \int_{-\infty}^{\infty} u dy dz$$

is a constant, independent of x (Batchelor 1967) and $\rho U_0 q$ is equal to the drag D on the obstacle. For the wake behind a surface-mounted obstacle in a turbulent shear flow this result no longer applies. CHJ argue that instead it is the moment of momentum flux deficit,

$$\tilde{C} = \int_0^{\infty} \int_{-\infty}^{\infty} z U_0(z) u dy dz, \quad (6)$$

which we will refer to as the "wake moment," that is a constant. For 2D obstacles we suppress the integral with respect to y and quantities are per unit cross-stream width. The wake moment is related, but not necessarily equal to the couple or overturning moment on the obstacle M. The difference between $\rho\tilde{C}$ and M is due to the pressure couple on the lower boundary and $\rho\tilde{C} > M$ (CHJ p. 552).

For both 2D and 3D obstacles we will work with coefficients normalized by an effective cross-stream width (w, set equal to 1 for 2D obstacles), an effective obstacle height h, and the upstream velocity at height h, $U_0(h)$. Normalized drag, couple, and wake moment coefficients are indicated by a subscript h and defined as

$$C_h = \frac{D}{1/2 \rho w h U_0^2(h)}, \quad (7)$$

$$M_h = \frac{M}{\rho w h^2 U_0^2(h)}, \quad (8)$$

and

$$\tilde{C}_h = \frac{\tilde{C}}{w h^2 U_0^2(h)}. \quad (9)$$

The factor 1/2 is retained in the definition of C_h, but omitted in the other definitions for consistency with most other authors. Beware however that some authors define drag and moment coefficients differently. Lemberg (1973) introduced the useful idea of the "centre of pressure," $h_p = M/D = 2hM_h/C_h$ with our notation. The actual determination of h and w may be a problem for irregularly shaped obstacles, for example, a tree. As a general rule, we would expect the frontal area to be approximately wh, but subjective adjustments could also be made in parallel estimations of $\tilde{C}_h$ or porosity.

Assuming that $\tilde{C}$ is a constant for the wake, as postulated by CHJ and featured in their theory, then we would like to use $\tilde{C}_h$ to characterize the wakes behind different 2D and 3D obstacles, even though information on its value for different obstacles may be hard to find or estimate. To provide guidance in estimating $\tilde{C}_h$, which will appear as a coefficient in our shelter model, we now review information on values of drag, couple, and wake moment coefficients.

a. 2D obstacles

In their conclusions, CHJ state that "for a general two dimensional obstacle there is no simple relation between the drag or couple on the obstacle and the wake flow." They do, however, give the result that for their study of flow past a 2D square block $\tilde{C}_h = 0.8$. Later wind tunnel results obtained by Castro (1979), again for 2D blocks of square cross section, confirm this result with values, based on matching wake profiles with the CHJ theory, ranging from 0.75 to 0.825. Castro also reports the couple on his obstacles and obtains values for M_h ranging from 0.16 to 0.28 with $h_p/h \approx 0.33$, whereas CHJ had roughly estimated their M_h value as 0.37. All are significantly less than $\tilde{C}_h$.

Castro's drag results for 2D blocks give C_h values of approximately 1.2 in two boundary-layer flows over

TABLE 1. Drag and moment coefficients from Lemberg's wind tunnel study. Results are calculated from Lemberg (1973, Table 5.5) assuming $U_h/U_0 = 0.8$ for $h = 4''$ and 0.84 for $h = 6''$. Boundary-layer depth, $\delta \approx 25''$. Models are, S4—4″ cube mounted normal to flow, S4D—4″ cube mounted diagonal to flow, C4—vertically mounted circular cylinder, 4″ diameter, 4″ height, S6—4″ × 4″ × 6″ (height) rectangular prism, mounted normal to flow, S6D—4″ × 4″ × 6″ (height) rectangular prism, mounted diagonal to flow, and C6—vertically mounted circular cylinder, 4″ diameter, 6″ height.

Model	S4	S4D	C4	S6	S6D	C6
C_h	0.85	0.73	0.45	0.88	0.76	0.48
M_h	0.33	0.30	0.19	0.33	0.30	0.19
h_0/h	0.76	0.82	0.83	0.76	0.78	0.80

his large block and 0.9 with a smaller block. The value of 1.2 is in good agreement with the drag coefficient for a 2D fence—see Taylor (1988) and as a rough guide *for 2D obstacles* we might expect $\tilde{C}_h = 2C_h/3$. For porous 2D obstacles or fences we can obtain a reasonable match with Perera's findings on the velocity deficit if we simply set

$$\tilde{C}_h = 0.8(1 - \varphi). \tag{10}$$

b. 3D obstacles

Lemberg (1973) tabulates drag, couple, and h_p/h results for a number of different 3D obstacles and we have used these results to compute the C_h and M_h values listed in Table 1. The C_h values differ slightly from those given in Taylor (1988) as a result of revised estimates of U_h. Compared to the values given above for 2D obstacles we find lower C_h values and, except for the cylinders, higher M_h values. For 3D obstacles the direct determination of $\tilde{C}_h$ would be difficult because of the need to collect and integrate velocity data across planes at several positions in the wake. Lemberg asserts, $\tilde{C}_h \approx M_h$, for 3D obstacles where the extent and magnitude of the pressure perturbations on the underlying surface upstream and downstream of the obstacle can be expected to be less than for 2D ones. This then implies $\tilde{C}_h \approx 0.3$ for "square" obstacles and 0.2 for vertical cylinders, with both values significantly lower than the value of 0.8 for 2D obstacles. We will use these as a first guess. Note that $h_p/h \approx 0.8$ for Lemberg's 3D obstacles, significantly higher than the 0.33 value found for 2D obstacles and implying that the force on these 3D obstacles is focused near the top. We suspect that this might not be the case for obstacles with a ridged or curved roof and that M_h might be lower in these cases. With the assumption that $\tilde{C}_h \approx M_h$ for Lemberg's 3D obstacles, we find that the ratio $\tilde{C}_h/C_h \approx 0.4$, somewhat lower than in the 2D case (0.66).

Although there have been other 3D wake studies—for example, the CSU work and those by Castro and Robins (1977), Sakamoto and Arie (1982), and Johnson and Surry (1987)—the study by Lemberg is the only one that we know of that gives data on the couple. Sakamoto and Arie studied pressure distributions on cubes of various sizes at various flow angles in a deep, smooth-wall, turbulent boundary layer. Their C_h results are compatible with Lemberg's and show a smooth transition with flow angle between normal and diagonal orientation. Johnson and Surry present results for the drag on hemispheres, domes, and tents. Typical C_h values range from 0.3 to 0.9 (Taylor 1988) but no data are available on the moment coefficients.

In Table 2 we summarize our estimates for C_h and $\tilde{C}_h$ for a variety of obstacles. It should be admitted that many of these are simply best guesses in the absence of data and that in all cases, especially for 3D obstacles, further study is highly desirable. Note that our estimates of $\tilde{C}_h$ for 3D obstacles are much lower than for 2D fences and that in this respect there is nonlinearity since the sheltering produced by a continuous 2D crosswind "fence" made up of an infinite series of cubical obstacles would be greater than the sum of the effects of the individual cubes. The lower $\tilde{C}_h$ values for 3D obstacles will lead to lower estimates of shelter effect than those predicted by WASP-SHELTER, which, in effect, appears to treat all obstacles as sections of 2D fence.

4. Previous approaches, WASP-SHELTER

The only model we are aware of that directly addresses the problem of estimating the sheltering produced by specified obstacles is the SHELTER module

TABLE 2. Suggested values for C_h and $\tilde{C}_h$ for various obstacle types.

Nature of obstacle	C_h	$\tilde{C}_h$	Comments
2D fences, or dense lines of trees	$1.2(1 - \varphi)$	$0.8(1 - \varphi)$	Note porosity adjustment
Long, low square buildings	1.0	0.25–0.4*	Ratios $w/h \geq 2$
3D cubical buildings	0.8	0.2–0.35*	$w/h \leq 2$
Vertical cylinder (silo)	0.5	0.2	
Hemisphere, with h averaged so that hw = frontal area	0.8	0.2	
Single or open lines of trees	0.4–0.8** × $(1 - \varphi)$	0.2–0.4** × $(1 - \varphi)$	Note porosity adjustment

* Use lower end of range for obstacles with a ridged or curved roof, upper end for flat-topped obstacles.
** Depending on foliage and shape.

of the WASP package developed by the Risø National Laboratory in Denmark. The user's guide to WASP 4.0 (Mortensen et al. 1993) describes the input required by SHELTER while Troen and Petersen's (1989) *European Wind Atlas* provides some details of the theory. Within WASP, obstacles are considered as boxes with a rectangular cross section. The user specifies the anemometer height, the surface roughness distribution, and the size and location of obstacles, such as buildings, trees, or fences, relative to the anemometer site. Mortensen et al. suggest including all obstacles that are less than $50h$ away, where h is the obstacle height, and for which the anemometer height z_A is less than $3h$. Warnings are given that the model estimates may not be realistic for sites very close to an obstacle. The DISPLAY option provides a map of the obstacle locations and WASP then estimates the expected sheltering at the anemometer for 30° sectors as a part of its wind analysis procedure.

Troen and Petersen (1989) describe how their SHELTER model is based on Perera's (1981) empirical formula for 2D fences and provide some guidance on the estimation of porosity. They (pp. 60, 85) provide simple expressions for the reduced shelter afforded by 3D compared to 2D obstacles but (p. 573) indicate that the procedure actually used in SHELTER involves the use of the 2D formula coupled to averaging over eight wind directions per 30° sector to simulate the lateral spread of wakes behind 3D obstacles. They also describe an adjustment for obstacles that are sufficiently close together so that one lies partially in the separation zone of the other. Results using WASP-SHELTER will be discussed below. We consider that the model probably overestimates the shelter provided by 3D obstacles.

There are several models that predict wake decay behind wind turbines and use this information to assist in the design of "wind farms." Examples are the PARK model supplied with the WASP package and based on work described by Katic et al. (1986), the AVENU Array model based on work by Lissaman et al. (1987) at AeroVironment, and the 2D model reported by Taylor (1980). There are some similarities between the type of sheltering calculations discussed in this paper and these models of wind turbine wakes, but the detailed assumptions are different, largely because turbines are elevated above ground and the wakes do not match the self-preserving forms associated with surface-mounted obstacles.

Wieringa (1976) also discusses sheltering effects. In this work the effects of upstream obstacles are represented by an increase in the effective roughness length z_0^{eff} for winds from those directions. Winds can then be adjusted to correspond to flow over a surface of standard roughness by assuming a uniform wind at a "blending height" of 60 m. The method uses measured gustiness to determine z_0^{eff} and there is no requirement for detailed information on the geometry of the obstacles. It is a different approach from that adopted here, and we should perhaps remark that for our model we are assuming $h \gg z_0$ so that there will be a clear distinction between the obstacle and the roughness elements.

5. The present model (WEMOD)

In this section we describe the basis for the algorithm used to compute shelter effects at an anemometer location. A computer code has also been developed.

a. Information required

The information needed for each obstacle is similar to that required by WASP-SHELTER and can be recorded on similar forms (Table 3). The differences from WASP are that we require ranges and angles of the extremities of the obstacle C_L, C_R (Fig. 1a) as seen from the anemometer site A, rather than the ranges and angles of the ends of the side facing the site

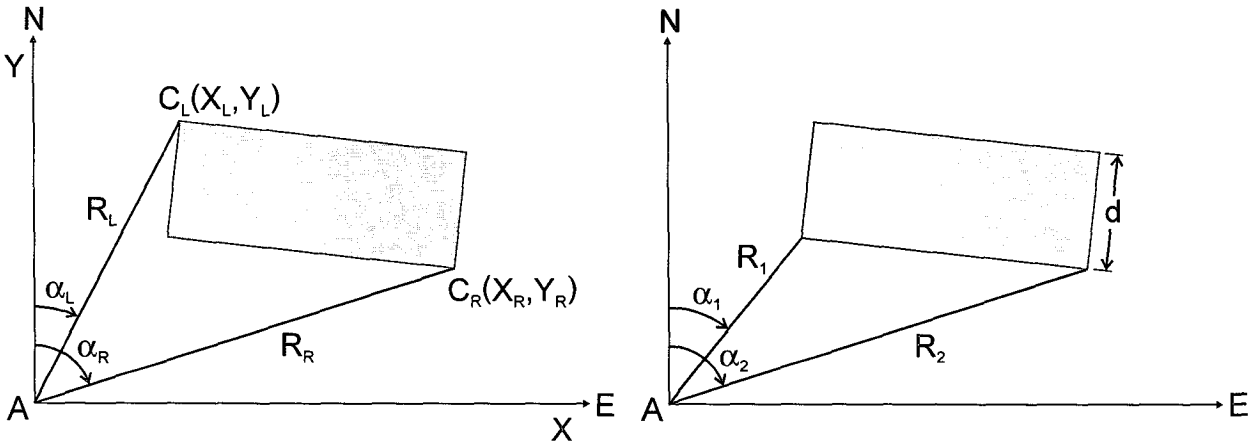

FIG. 1. (a) Definition diagram for obstacles in present format. (b) Definition diagram for obstacles with WASP format.

[Fig. 1b–c.f. Mortensen et al. (1993), Fig. 12]. We consider this to be preferable for irregularly shaped obstacles and also note that there will be no direct dependence on estimates of the depth d of rectangular obstacles. We refer to our left and right ranges and angles to the points C_L and C_R as (R_L, α_L) and (R_R, α_R). We assume that 1° resolution will normally suffice for this specification. For a truly infinite fence or line of trees there is a problem with either scheme if the points C_L and C_R are identified as points 180° apart at infinity and we cannot determine the distance between the fence and the anemometer. Fences subtending an angle greater than about 120° should be specified as two separate sections to avoid this problem.

For each obstacle we require a good estimate of height h and as discussed above in section 3 we must estimate a wake moment coefficient $\tilde{C}_h$ from information on the shape and possibly the orientation of the obstacle. Some guidelines are given in Table 2. For shelterbelts, trees, and fences, we require an estimate of the porosity φ defined for a 2D fence as the ratio of open area to total frontal area, in order to estimate $\tilde{C}_h$. If an obstacle has a wide variation in height from one section to another it may be appropriate to consider it as composed of several component obstacles. If, however, two or more obstacles are in line upwind of the anemometer site and close or moderately close together (say within $15h$ for 2D obstacles or $5h$ for 3D obstacles) then linear superposition will overestimate sheltering effects and some adjustments may be called for. In practice we sometimes ignore the smaller of two upwind aligned obstacles or combine them as a single, equivalent obstacle. Bear in mind that the model is only *estimating* shelter effects and one should be prepared to conduct tests of the sensitivity to input assumptions as appropriate.

b. Geometrical considerations and relationships

We plan to consider each complete single obstacle as a series of plane, vertical, and rectangular barrier segments of height h, placed normal to the wind as indicated in Fig. 2. The wind direction is denoted by ψ. Each of these segments will represent that portion of the obstacle subtending 1° at A and will be centered on the angle β_i, for which we will take values $\alpha_L + 0.5°$, $\alpha_L + 1.5°$, ... $\alpha_R - 0.5°$. The range from A to the center of the ith barrier segment will be

$$R = \frac{X_R Y_L - X_L Y_R}{(X_R - X_L)\cos\beta_i - (Y_R - Y_L)\sin\beta_i}, \quad (11)$$

where $(X_L, Y_L) = (\sin\alpha_L, \cos\alpha_L)R_L$ and $(X_R, Y_R) = (\sin\alpha_R, \cos\alpha_R)R_R$ are the X, Y coordinates of C_L and C_R in the usual geographic Cartesian frame with the origin at A and with the X axis pointing toward the east. We denote the angle made by the normal to the line C_LC_R with true north by γ. This will be given by $\tan\gamma = (Y_L - Y_R)/(X_R - X_L)$, with the 180° ambiguity resolved by consideration of the sign of $(X_R - X_L)$. The width of this model barrier segment (which is considered to be aligned normal to the wind direction) will then be given, approximately, by

$$w = 2R \sin 0.5° \sec(\beta_i - \gamma)|\cos(\psi - \gamma)|. \quad (12)$$

This expression gives the projection, on a line normal to the wind direction, of the length of that portion of line C_LC_R centered at angle β_i and subtending 1° at the anemometer location.

In a second Cartesian frame of reference, with coordinates given as lowercase letters (x, y) centered at the middle of the base of barrier segment i and with the x axis aligned with the flow, the location of A (see Fig. 3) will be

$$(x, y) = [R\cos(\psi - \beta_i), R\sin(\psi - \beta_i)]. \quad (13)$$

These distances provide the basic geometry for the wake velocity deficit calculations presented below.

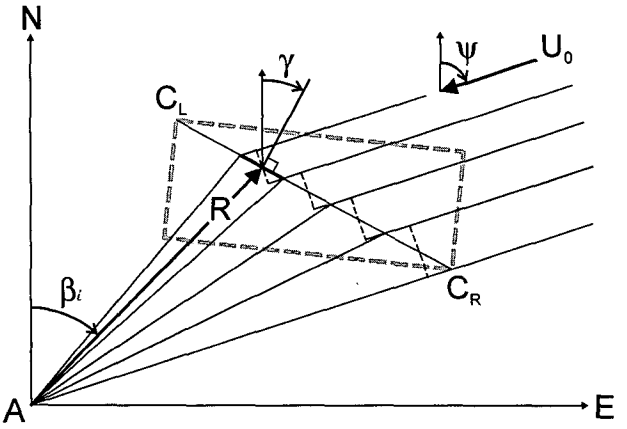

FIG. 2. Representation of an obstacle by a series of rectangular wind breaks (plan view). Thick dashed line is the outline of the original obstacle. The solid line is the portion of the line C_LC_R subtending 1° at A, centered on angle β_i (1° angle is exaggerated). The thin dashed line is the equivalent barrier normal to the wind.

c. Speed reduction due to single and multiple obstacles for a specified wind direction

The first step is to calculate the relative velocity reduction at A corresponding to the effect of an upwind component barrier i of obstacle n. We will designate this by $u_{n,i}$. For component barriers downwind (in a 180° sense) of the anemometer, the velocity reduction is taken to be zero. Following Perera (1981) and others, the velocity perturbation will be given in terms of $U_0(h)$ initially, and we will make a further adjustment to scale with $U_0(z_A)$. The basic velocity reduction is computed from

$$\frac{u_{n,i}}{U_0(h)} = \Gamma\tilde{C}_h\left(\frac{w}{h}\right)\left(\frac{x}{h}\right)^{-1.5} F(\eta)G(\xi), \quad (14a)$$

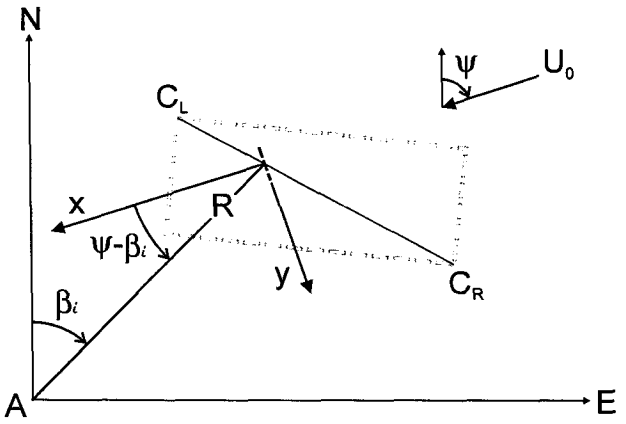

FIG. 3. The (x, y) location of A relative to a component barrier for wind direction ψ.

where $\eta = (y/h)(x/h)^{-1/2}$ and $\zeta = (z/h)(x/h)^{-1/2}$. The coefficient Γ will be discussed below. There are no adjustments made to allow for a virtual origin, in agreement with Lemberg's (1973) observations, and x is simply the distance downwind from the component barrier.

The function F represents the lateral spread of the wake. As discussed above in section 2 we assume a Gaussian spread, given by

$$F(\eta) = \frac{1}{(2\pi)^{1/2} a_f} \exp\left(\frac{-\eta^2}{2a_f^2}\right), \qquad (14b)$$

where a_f is a parameter whose normal recommended value (see section 2) is 0.5. Tests with different values for a_f will be briefly discussed below in section 6. Because of the representation of obstacles by 1° barrier segments the model would give erroneous results for small (<0.05) values of a_f.

The function G is based on Perera's empirical formula for 2D obstacles but with n, the power-law exponent of the approach flow velocity profile, assumed small compared to 2. The formulation is then

$$G(\zeta) = c_a \zeta \exp(-a_g \zeta^{1.5}). \qquad (14c)$$

Coefficients c_a and a_g are h dependent based on Perera's expressions but neglecting any zero plane displacement d and adding z_0 to h. They are,

$$c_a = \left\{\frac{\ln[(h + z_0)/z_0]}{2\kappa^2}\right\}^{1/2} \quad \text{and} \quad a_g = 0.67 c_a^{1.5}, \qquad (14d)$$

with $\kappa = 0.4$.

When these formulas for 3D component barriers are integrated or summed for a 2D fence normal to the flow then we recover the Perera result in the form,

$$\frac{u}{U_0(h)} = \Gamma \tilde{C}_h \left(\frac{x}{h}\right)^{-1} G(\zeta). \qquad (15)$$

Substituting this expression into Eq. (6) for $\tilde{C}$, and integrating, with the approximation $U_0(z) \approx U_0(h)$, which is linked to our assumption that $(n+2)^{-1} \approx 0.5$, we obtain $\Gamma = 0.67 c_a^2$. For typical values of $h/z_0 = 10^2$ and 10^3, this gives $\Gamma = 9.7$ and 14.3, respectively. If, however, we assumed Γ to be a universal constant, in keeping with Perera's approach, then, for agreement with his results and given our basic $\tilde{C}_h$ of 0.8 for a 2D solid obstacle, the required value would be $\Gamma = 12.2$. Another way to look at this would be to argue that, for a given obstacle placed on surfaces with different roughnesses, $\tilde{C}_h$ should, strictly speaking, vary with h/z_0. To avoid this additional complication and to retain conformity with the Perera model for 2D obstacles we will simply set $\Gamma = 12.2$. Given the uncertainties likely in estimates of $\tilde{C}_h$ this seems the most practical approach for the present time.

Finally, the adjustment to scale with $U_0(z_A)$ gives

$$s_{n,i} = \frac{u_{n,i}}{U_0(z_A)} = \frac{u_{n,i}}{U_0(h)} \frac{\ln[(h + z_0)/z_0]}{\ln[(z_A + z_0)/z_0]}, \qquad (16)$$

assuming a log profile with roughness z_0. The overall effect of obstacle n is given by $S_n = \sum s_{n,i}$, summed over i. The final stage, for wind direction ψ, is to add the effects of all single obstacles, assuming a linear process. This implies that we are in the far wake of all of the obstacles and that this linear superposition also applies to the situation where one obstacle lies in the wake of another—but see the discussion in section 5a. The summation gives the relative reduction in the wind speed at height z_A for direction ψ caused by all of the obstacles identified by the shelter survey. In our basic model code this quantity is calculated at 1° intervals between 0° and 360° to define the shelter effect for any wind direction.

6. Sample calculations and comparisons with other work

As an initial test of our model we performed calculations for 2D fences and compared them with Perera's (1981) wind tunnel cases and with his empirical formula. Perera's wind tunnel study had $h/z_0 \approx 100$ and he presents results for solid and porous fences. The power-law exponent n is not given, but for the simulated rural boundary-layer case that he describes the value is probably about 1/7. We have assumed $n \approx 0$ in applying Perera's empirical formula. The errors involved will be small (~5%).

In Fig. 4a we compare our simple model predictions with Perera's results (extracted from his Fig. 2) for the velocity reductions at differing downwind distances and at height $h/2$ in the flow behind a slightly porous fence with $\varphi = 0.1$. The incident flow is normal to the fence. The modeled velocity reductions (using $z_0 = 0.1$ m, $h = 10$ m, and $z_A = 5$ m as representative full-scale equivalents to Perera's model values) are generally in fair agreement with the tunnel data although they ap-

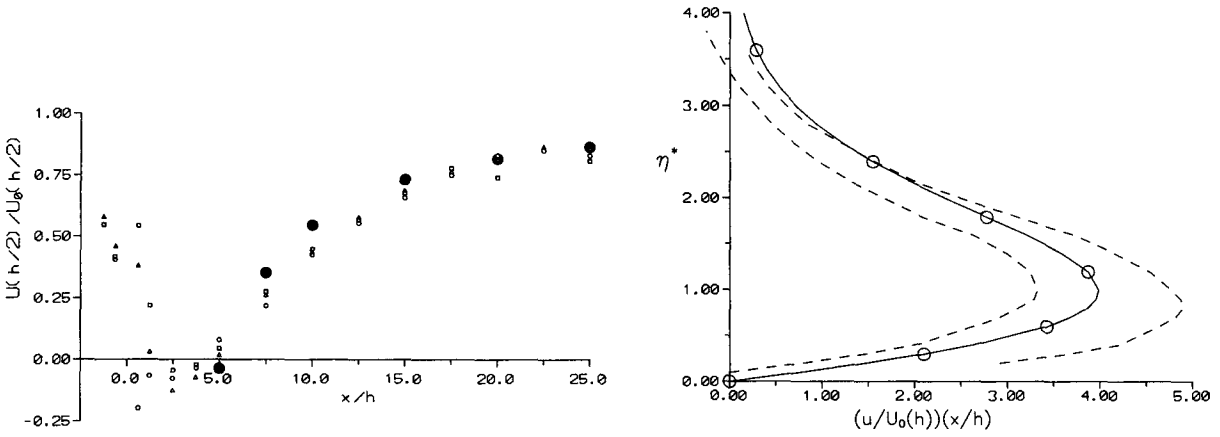

FIG. 4. (a) Modeled (●) downstream variation of the wind at height $h/2$ behind an infinite 2D fence of porosity 0.1. Data (small symbols) are from Perera (1981) for fences with different forms of construction. (b) Vertical variation of velocity deficit behind an infinite 2D fence of porosity 0.2 (——, Perera formula, O, WEMOD calculation). Measurement range (-----) indicated is based on data from Perera (1981) at downstream distances between $7.5h$ and $25h$. One or two outlying points have been excluded. The vertical coordinate is $\eta^* = (z/h)(x/h)^{-1/2}c_a$ with $c_a = 3.80$ in this case.

pear to underestimate the velocity reductions at $x/h = 7.5$ and 10.0. In this region, however, the observed velocity reductions are large (>50%), and we would not generally expect to find anemometer sitings subject to such severe sheltering. As a general rule we would be cautious about wind data where the sheltering estimate exceeded 30%. We used this test case to confirm that the model output was independent of the orientation of the obstacle provided it remained in the same position relative to the anemometer location, independent of absolute length scale, and that fences could be treated as being made up of several segments. We also confirmed that the shelter results downwind of a 2D fence aligned normal to the wind were independent of a_f (for $0.1 < a_f < 1.0$). Note that for wind at an angle to the fence, there will still be a weak dependence on a_f.

Figure 4b shows the predicted vertical variation in the velocity reduction behind a $\varphi = 0.2$ fence and includes an indication of the spread of Perera's data (extracted from his Fig. 5b) for $7.5 < x/h < 25$. Again we assume $n \approx 0$ in relating Perera's and our vertical coordinate. As indicated above, our formulation is based directly on Perera's empirical formula and matches it exactly for these 2D cases. Neither the Perera formula nor our model include an allowance for the small velocity increases (negative u) at the outer edge of the wake although these are frequently observed. Note that in this figure we have plotted $u/U_0(h)$ rather than scaling with $U_0(z_A)$.

In Fig. 5 we illustrate the predictions of our model for the sheltering effect on 5-, 10-, and 20-m winds caused by an infinite, 5-m-high solid fence aligned north–south at a distance of 100 m to the west of an anemometer site, which has a roughness length z_0 of 0.03 m. These results were generated by considering the fence as two semi-infinite fences extending to the north and south of the point 100 m due west of the anemometer site. Identical results were obtained for $220° < \psi < 320°$ when the obstacle was a single fence at the same distance but limited to the sector from 210° to 330°. The wind speed reduction is plotted as a function of wind direction. For anemometer heights of 5 and 10 m there is a steady reduction from maxima of 0.25 and 0.15, respectively, as the wind direction moves away from being normal to the fence, while for a height of 20 m at a distance of 100 m from the fence there are maxima when the flow is from about 200° or 340°, almost parallel to the fence. This arises because the anemometer is in the very outer portion of the wake at normal incidence. At shallow angles to the fence, the effective downwind distance is increased; the

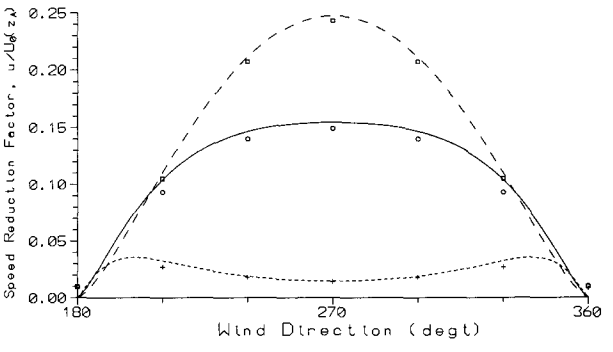

FIG. 5. Sheltering effect on 5-, 10-, and 20-m winds caused by an infinite, 5-m-high solid fence aligned north–south at a distance of 100 m to the west of an anemometer site with $z_0 = 0.03$ m. The wind speed reduction is plotted as a function of wind direction. Lines indicate WEMOD estimates, while symbols are WASP-SHELTER results (- - -, □, $z_A = 5$ m), (——, O, $z_A = 10$ m), and (-----, +, $z_A = 20$ m).

maximum velocity reduction will be lower but the wake will be deeper. Results obtained with the SHELTER module of WASP 4.0 are also shown. WASP-SHELTER results are averages for 30° sectors but give very similar results to WEMOD, as expected since both use Perera's results as a basis.

For 3D obstacles we have made comparisons with selected wind tunnel data reported by Lemberg (1973) and Castro and Robins (1977) and with Colmer's (1971) field study of the wake behind a hangar. With $a_f = 0.5$ and with $\tilde{C}_h$ values selected from Table 2 there is generally good agreement in all cases with $x/h \geq 3$, as we should expect since the model was to some extent tuned with these data. Note that we can use the model for sites much closer to 3D obstacles than for 2D fences. Results for velocity reduction downstream of Lemberg's S4 cube (4″ sides, aligned normal to flow) are presented in Fig. 6, where we have taken $\tilde{C}_h = 0.35$ in the WEMOD calculations. The wind tunnel data have been extracted from Lemberg's Figs. 5–6 and 5–13. In Fig. 6a we show the (centerline) variation of the wind speed reduction u as a function of x, directly downstream of the center of the cube at three heights. The lateral spread is illustrated in Fig. 6b, which shows u as a function of the wind direction relative to the vertical plane containing the center of the obstacle and the anemometer. The WEMOD results correspond to $z_A = 0.5h$ and are for anemometer locations $4.5h$, $6.8h$, and $9.3h$ distance from the cube. Lemberg's data are for approximately the same situation but with small variations in the obstacle to anemometer distance due to the different geometries considered. As indicated above in section 2 there is considerable scatter in Lemberg's wind tunnel data for both downwind decay and lateral spread. Bearing this in mind, the agreement between the WEMOD estimates and the tunnel data can be considered as satisfactory. Note that for these obstacles there may be slight errors introduced by WEMOD because angles are only specified to the nearest whole degree. We avoided this problem in Fig. 6a by judicious selection of the x/h values for which calculations were made but 5% obstacle width errors were present in the calculations made for Fig. 6b. WASP-SHELTER calculations for the cases illustrated in Fig. 6b give $u/U_0(z_A)$ values of 0.32, 0.21, and 0.11 at 0° and 0.00 at 30° for the three x/h ranges depicted. For 0° the $u/U_0(h)$ values are 0.29, 0.19, and 0.10, roughly double those given by WEMOD. In this context the basic difference between WEMOD and WASP-SHELTER is that WEMOD reduces the impact of 3D obstacles compared to 2D ones through the $\tilde{C}_h$ coefficient, while WASP-SHELTER does not. One way for a user to effect this reduction within the WASP-SHELTER model would be to specify a porosity of order 50% for 3D obstacles.

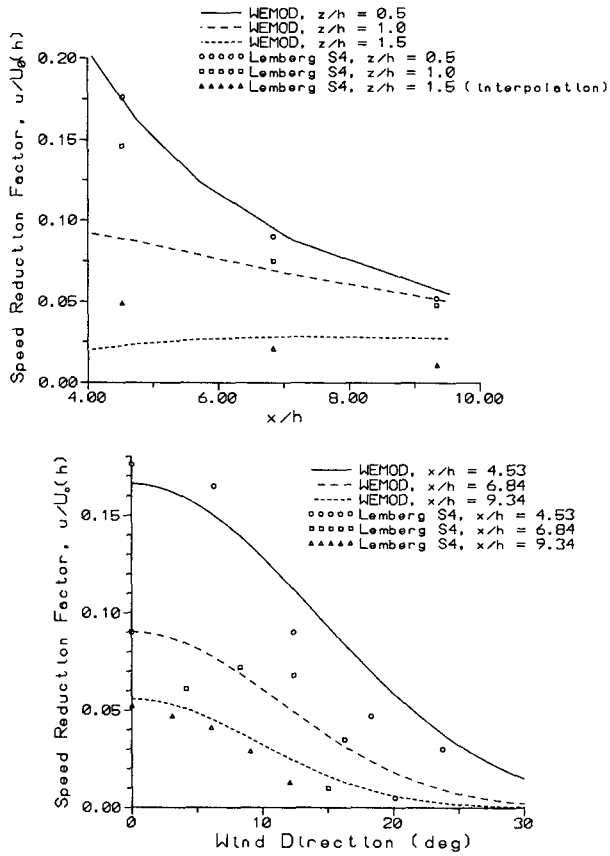

FIG. 6. Comparisons with Lemberg's wind tunnel study of the wake behind a cube normal to the flow—the S4 case. (a) Wind speed reductions $[u/U_0(h)]$ directly downwind of the obstacle at $z = h/2$, h, and $3h/2$. (b) Wind speed reductions $[u/U_0(h)]$ at three downwind locations as a function of the wind direction relative to the line between the center of the base of the obstacle and the measurement location, $z = h/2$.

For Colmer's (1971) study of the wake behind a 10-m-high, 30-m-wide, and 15-m-deep hangar, we estimated $z_0 = 0.035$ m by plotting his upstream velocity data and have taken a relatively low value of $\tilde{C}_h = 0.2$ to account for the pitched roof, which may have a partial streamlining effect. Colmer's data are quite limited and show wind speed increases for some locations with $z > h$. The most appropriate comparisons are for anemometer locations directly downwind of the hangar at $x = 54$ m, $y = 0$ m, and $z = 3$ m and 9 m and at $x = 144$ m, $y = 0$ m, and $z = 9$ m, where Colmer's measured values of $u/U_0(z_A)$ are 0.12, 0.14, and 0.03, respectively. Our predictions are 0.20, 0.15, and 0.05. Thus, even with a relatively low value of $\tilde{C}_h$, we still appear to overestimate these velocity reductions. The model predictions would be reduced with a higher value of a_f, but we are reluctant to revise this without additional data. The WASP-SHELTER model (version 4.0) overestimates the shelter effect in this case with reductions of 0.69, 0.66, and 0.14 at the three locations discussed above.

As an illustration of the use of WEMOD for sites with a number of obstacles, we consider the anemom-

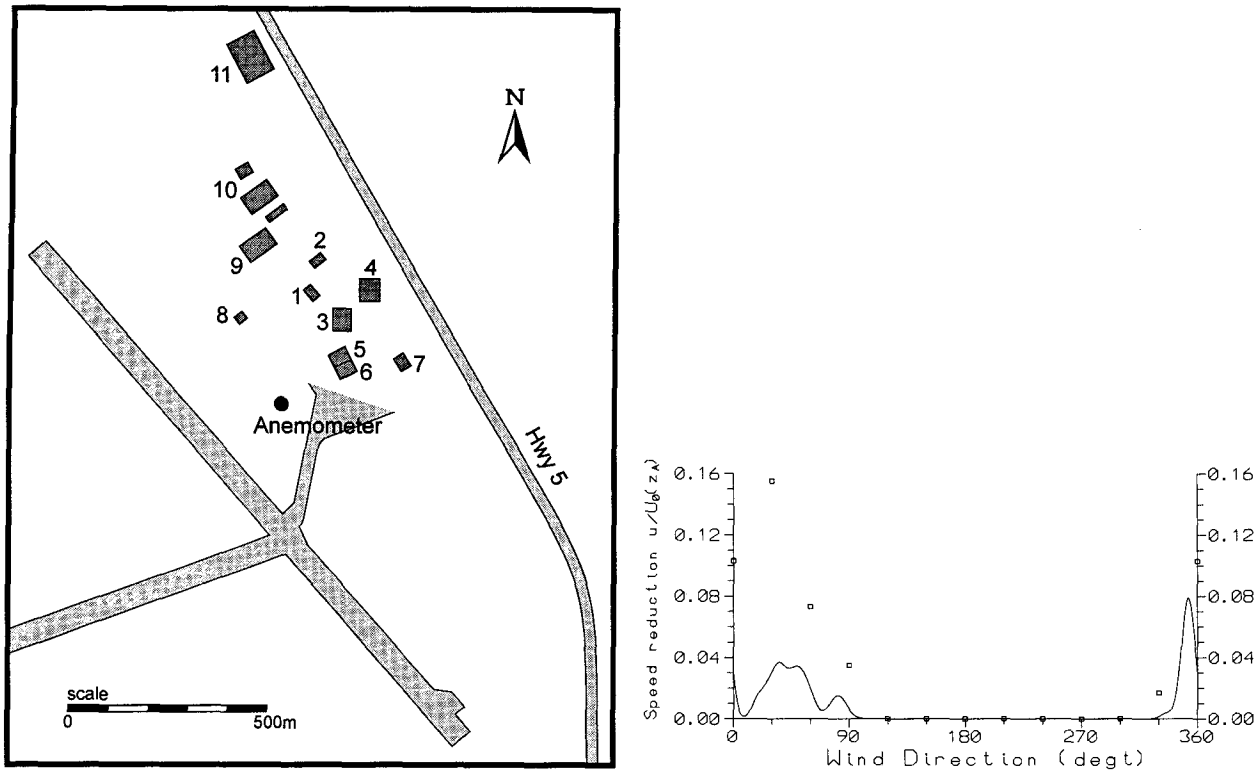

FIG. 7. Shelter corrections for the AES anemometer at Lethbridge Airport as a function of wind direction (°T). (a) Sketch map of the site, not to scale. Numbers refer to buildings on the obstacle description form. (b) Wind speed reduction calculations using WEMOD (1° resolution, ——) and WASP (30° sectors, □).

eter at Lethbridge Airport (Alberta). A sketch map of the anemometer location is given in Fig. 7a, while Table 3 is the obstacle description form, based on a mix of in situ site measurements plus study of the airport plan. The sheltering factors predicted by WEMOD and WASP are shown as a function of wind direction (°T) in Fig. 7b. We should remark first that, as is typical for airport installations, the anemometer has good exposure in all directions and no obstacles were reported for angles between 83° (the Flying Club hangar) and

TABLE 3. Obstacle description form. Station: Lethbridge Airport; date: 9 November 1992; surface type: mostly short grass; Z_0 = 0.02 m magnetic to true direction correction applied, +21°.

Number	α_L	R_L	α_R	R_R	h	Obstacle type and porosity, assumed zero if not given	$\tilde{C}_h$
1	015	290	017	280	5.3	West Wind building	0.20
2	018	348	019	360	3.7	Unidentified building	0.25
3	022	244	026	225	9.5	Time Air building	0.25
4	031	320	039	325	9.5	Armories, estimated	0.25
5	042	120	046	117	7.0	Terminal, northern half	0.25
6	046	117	062	114	3.5	Terminal, southern half	0.30
7	080	246	083	252	13.4	Lethbridge Flying Club	0.25
8	335	276	336	276	6.1	Fire Hall building	0.30
9	346	434	357	405	10.7	Triple E S. building	0.35
10	349	525	358	525	10.7	Triple E N. building, estimated	0.35
11	351	850	358	840	9.1	Regent Homes building, estimated	0.35

Angles α in degrees true from north, ranges R, and heights h, in meters.

Additional information: Two small buildings northwest and southeast of obstacle number 10 have been omitted on the grounds that they are close to obstacles 9 and 10 and will not add significantly to the sheltering caused by those obstacles.

Observers: Ross Dickinson and Peter Taylor.

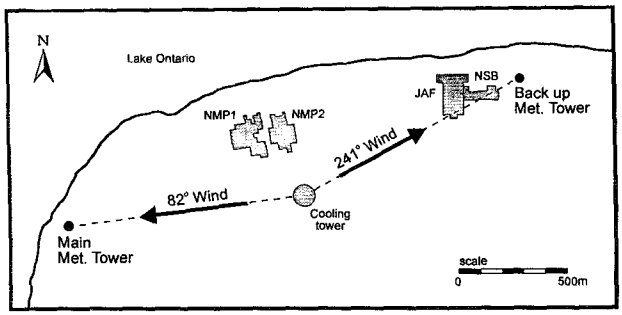

FIG. 8. Site map and building locations at the James A. Fitzpatrick Nuclear Power Station (after Meroney et al. 1988).

335° (the Fire Hall). The roughness length was taken as 0.02 m. The maximum estimated wind speed reductions from WEMOD are about 3.5% at 30°–45° due to the Time Air (3) and Terminal Buildings (5, 6) and the Armories (4) behind them, as well as a narrow peak of almost 8% at 353° due to the Triple E (9, 10) and Regent Homes (11) buildings. For this site, WASP-SHELTER predicts a 15.5% reduction for the 30° wind direction and 10.3% for winds from due north.

As a further example of the type of situation in which WEMOD could be applied we have made estimates of the sheltering due to generator buildings and a cooling tower for winds from 82° and 241° at heights of 10, 30, and 60 m on two meteorological towers installed at the James A. Fitzpatrick Nuclear Power Station (Fig. 8). This situation has been studied in the wind tunnel by Meroney et al. (1988) (see also Shin et al. 1990), and our calculations were made for comparison with their simulations. The WEMOD estimates were compatible with the high-speed wind tunnel results for both the main and backup tower locations in the sense that both predict only small additional sheltering effects due to the installation of the cooling tower (<4%) and the new services building (<6%). The simple assumptions made in WEMOD will lead to smoother results and cannot reproduce the complex behavior, such as wind increases (−ve shelter), observed in the wind tunnel at some levels. For winds from 241° there is substantial overall sheltering at the backup tower (≈20%) due primarily to the JAF reactor building.

7. Conclusions

From a review of wind tunnel and field observations of the mean wind in the wake behind 2D and 3D obstacles, it is clear that velocity perturbations are approximately self-preserving in the far wake region and that the wake moment is approximately conserved, as argued by CHJ. It is also apparent that the wake moment coefficient $\tilde{C}_h$ is significantly smaller for 3D obstacles than for 2D fences. This difference is not accounted for in the WASP-SHELTER model and, in our view, leads to a significant overestimation of the sheltering behind 3D obstacles. The WEMOD model presented here is, like WASP, based on Perera's (1981) empirical formula for 2D wakes. It assumes a Gaussian crosswind spread for 3D obstacles and computes shelter effects at 1° resolution. In WEMOD $\tilde{C}_h$ is a parameter that the user must specify for each obstacle and with suitable selection of $\tilde{C}_h$ the model is shown to produce results that match available observational data. As typical applications of the model we estimated the sheltering effects of buildings at Lethbridge Airport (Alberta, Canada) and the J. A. Fitzpatrick Nuclear Power Station (New York State) on wind measurements at those sites.

We consider the model proposed here as a relatively simple one. For instance we have used approximated power-law coefficients (0.5, 0.5, 1.5) and a single c_f value of 0.5 and the $\tilde{C}_h$ coefficient is probably only known for most 3D obstacles to within about 50%. We have also used a single surface roughness value for all wind directions. With more data these might be refined or improved but we would contend that the model already provides a reasonable first estimate in most cases. A useful step to improving model estimates would be to conduct further field and/or wind tunnel studies to obtain $\tilde{C}_h$ values for a range of obstacle shapes.

Acknowledgments. This work was prompted by the requirements of a wind energy study (project SWI/90/8-1) conducted under the auspices of the South West Alberta Renewable Energy Initiative. We are grateful for the support and encouragement of Mary Ellen Jones in relation to that project. Eric Petersen of the Risø National Laboratory in Denmark kindly provided us with the latest version of WASP, Transport Canada provided a site map of Lethbridge airport, and Robert Meroney provided additional details of the CSU wind tunnel study of the J. A. Fitzpatrick site. Some programming and plotting were done by Steven Lamming and Paul Stalker of Zephyr North.

REFERENCES

Arya, S. P. S., and M. S. Shipman, 1981: An experimental investigation of flow and diffusion in the disturbed boundary-layer over a ridge. I: Mean flow and turbulence structure. *Atmos. Environ.*, **15**, 1173–1184.

——, and P. S. Gadiyaram, 1986: An experimental study of flow and dispersion in the wakes of three-dimensional low hills. *Atmos. Environ.*, **20**, 729–740.

Batchelor, G. K., 1967: *An Introduction to Fluid Dynamics.* Cambridge University Press, 615 pp.

Castro, I. P., 1979: Relaxing wakes behind surface mounted obstacles in rough-wall boundary layers. *J. Fluid Mech.*, **93**, 631–659.

——, and A. G. Robins, 1977: The flow around a surface-mounted cube in uniform and turbulent streams. *J. Fluid Mech.*, **79**, 307–335.

Colmer, M. J., 1971: Some full-scale measurements of the flow in the wake of a hangar. Aeronautical Research Council (UK) Current Paper, C.P. No. 1166 HMSO London, 13 pp + figures.

Counihan, J., J. C. R. Hunt, and P. S. Jackson, 1974: Wakes behind

two dimensional obstacles in turbulent boundary-layers. *J. Fluid Mech.*, **64,** 529–563.

Hanna, S. R., G. A. Briggs, and R. P. Hosker, Jr., 1982: *Handbook on Atmospheric Diffusion.* U.S. Dept. of Energy, DOE/TIC 11223, 102 pp.

Hansen, A. C., and J. E. Cermak, 1975: Vortex-containing wakes of surface obstacles, Project THEMIS Tech. Report, CER75-76ACH-JEC16, 163 pp. [Available from College of Engineering, Colorado State University, Fort Collins, CO 80523.]

Hosker, R. P., Jr., 1984: *Flow and Diffusion Near Obstacles. Atmospheric Science and Power Production,* D. Randerson, Ed., U.S. Dept of Energy, 241–326.

Hunt, J. C. R., 1971: The effect of single buildings and structures. *Phil. Trans. Roy. Soc. London, Ser A,* **269,** 457–467.

——, 1974: Wakes behind buildings. Paper presented at Aeronautical Research Council (UK) Atmospheric Environment Committee Meeting, London, England, ARC Report 35601, Atmos 229.

Johnson, G. L., and D. Surry, 1987: Unsteady wind loads on tents. Boundary Layer Wind Tunnel Report, BLWT-SS5-1985, University of Western Ontario, London, Ontario, Canada.

Katic, I., J. Højstrup, and N. O. Jensen, 1986: A simple model for cluster efficiency. *Proc. European Wind Energy Association Conf. and Exhibition,* Rome, 407–410.

Kothari, K. M., J. A. Peterka, and R. N. Meroney, 1979: Stably stratified building wakes. Report CER78-79KMK-JAP-RNM65, 143 pp. [Available from Dept of Civil Engineering, Colorado State University, Fort Collins, CO 80523.]

Lemberg, R., 1973: On the wakes behind bluff bodies in a turbulent boundary-layer. Ph.D. thesis Report No. BLWT-3-1973, University of Western Ontario, Boundary Layer Wind Tunnel Laboratory, London, Ontario, Canada.

Lissaman, P. B. S., D. R. Foster, and B. D. Hibbs, 1987: Operational model for the design of optimum wind farm arrays. Report AV-FR-86/837R, AeroVironment Inc., Monrovia, California, prepared for U.S. Dept of Energy, Washington, D.C., Contract DE-AC03-896-ER80422.

Meroney, R. N., R. L. Ewald, S-H. Shin, and D. E. Neff, 1988: Wind-tunnel studies of certain meteorological tower siting characteristics at the James A. Fitzpatrick nuclear power station. Final Report to New York Power Authority, CSU Contract No. 2-96920, 72 pp. [Available from College of Engineering, Colorado State University, Fort Collins, CO 80523.]

Mortensen, N. G., L. Landberg, I. Troen, and E. L. Petersen, 1993: Wind atlas analysis and application program (WASP)—User's Guide, Risø-I-666(EN), Risø National Laboratories. [Available from Risø National Laboratories, P.O. Box 49, DK-4000, Roskilde, Denmark.]

Perera, M. D. A. E. S., 1981: Shelter behind two dimensional solid and porous fences. *J. Wind Eng. Industr. Aerodyn.*, **8,** 93–104.

Sakamoto, H., and M. Arie, 1982: Flow around a cubic body immersed in a turbulent boundary-layer. *J. Wind Eng. Industr. Aerodyn.*, **9,** 275–293.

Salmon, J. R., 1987: MS-Micro Users Guide. Final report of Contract 01SE-KM147-4-2982 to Environment Canada, Atmospheric Environment Service. [Available from Atmospheric Environment Service, 4905 Dufferin St., Downsview, Ontario, Canada M3H 5T4 (Attn., John Walmsley).]

Seginer, I., and R. Sagi, 1972: Drag on a windbreak in two-dimensional flow. *Agric. Meteorol.*, **9,** 323–333.

Shin, S-H, R. N. Meroney, R. L. Ewald, and D. E. Neff, 1990: Effect of upwind obstacles and meteorological tower structure on sensor measurements. *J. Wind Eng. Industr. Aerodyn.*, **36,** 371–379.

Taylor, P. A., 1980: On wake decay and row spacing for WECS farms. *Proc. Third Int. Symp. on Wind Energy Systems,* BHRA Fluid Engineering, Cranfield, 451–468.

——, 1988: Turbulent wakes in the atmospheric boundary-layer. *Proc. Int. Symp. on Flow and Transport in the Natural Environment: Canberra 1987,* W. L. Steffen and O. T. Denmead, Eds., Springer, 270–292.

Townsend, A. A., 1965: The response of a turbulent boundary layer to abrupt changes in surface conditions. *J. Fluid Mech.*, **22,** 799–822.

Troen, I., and E. L. Petersen, 1989: *European Wind Atlas.* Risø National Laboratory, 656 pp.

Wieringa, J., 1976: An objective exposure correction method for average wind speeds measured at a sheltered location. *Quart J. Roy. Meteor. Soc.*, **102,** 241–253.

Woo, H. G. C., J. A. Peterka, and J. E. Cermak, 1976: Wind tunnel measurements in the wakes of structures. Report CER75-76-HGCW-JAP-JEC40. [Available from Colorado State University, Fort Collins, CO 80523.]